Check for updates

OPEN

Statistical modeling and optimization of heterogeneous Fenton-like removal of organic pollutant using fibrous catalysts: a full factorial design

Mohammad Neaz Morshed[1,2,3,4]✉, Md. Nahid Pervez[5], Nemeshwaree Behary[2,3], Nabil Bouazizi[2], Jinping Guan[4] & Vincent A. Nierstrasz[1]

This work focuses on the optimization of heterogeneous Fenton-like removal of organic pollutant (dye) from water using newly developed fibrous catalysts based on a full factorial experimental design. This study aims to approximate the feasibility of heterogeneous Fenton-like removal process and optionally make predictions from this approximation in a form of statistical modeling. The fibrous catalysts were prepared by dispersing zerovalent iron nanoparticles on polyester fabrics (PET) before and after incorporation of either polyamidoamine (PAMAM, $-NH_2$) dendrimer, 3-(aminopropyl) triethoxysilane (APTES, $-Si-NH_2$) or thioglycerol (SH). The individual effect of two main factors [pH (X1) and concentration of hydrogen peroxide-$[H_2O_2]_{\mu l}$ (X2)] and their interactional effects on the removal process was determined at 95% confidence level by an L^{27} design. The results indicated that increasing the pH over 5 decreases the dye removal efficiency whereas the rise in $[H_2O_2]_{\mu l}$ until equilibrium point increases it. The principal effect of the type of catalysts (PET–NH_2–Fe, PET–Si–NH_2–Fe, and PET–SH–Fe) did not show any statistical significance. The factorial experiments demonstrated the existence of a significant synergistic interaction effect between the pH and $[H_2O_2]_{\mu l}$ as expressed by the values of the coefficient of interactions and analysis of variance (ANOVA). Finally, the functionalization of the resultant fibrous catalysts was validated by electrokinetic and X-ray photoelectron spectroscopy analysis. The optimization made from this study are of great importance for rational design and scaling up of fibrous catalyst for green chemistry and environmental applications.

Detoxification of wastewater is a great challenge due to the presence of toxic, complex and diverse organic pollutants that resistant to conventional treatment systems consists of an either-or combination of physical, chemical, and biological processes[1–4]. Advance process such as adsorption, ozone and/or hypochlorite oxidation is effective but undesirable due to their inherent drawback related to cost, efficiency and generation of secondary waste[5–7].
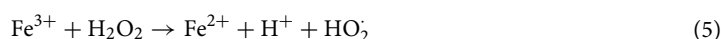
Recent progress in the removal of toxic pollutants has led to the development of advanced oxidation processes (AOPs). Among them, the oxidation using Fenton's reagent has proved to be a promising and attractive treatment method for its effectiveness towards the destruction of a large number of hazardous and organic pollutants[8,9]. The Fenton process uses iron ions and hydrogen peroxide for the generation of the second most powerful oxidant, i.e., hydroxyl radicals in aqueous solution[10,11] which is capable of mineralizing organic pollutants in various

[1]Textile Material Technology, Department of Textile Technology, Faculty of Textiles, Engineering and Business, University of Borås, 50190 Borås, Sweden. [2]Ecole Nationale Supérieure des Arts et Industries Textiles (ENSAIT), GEMTEX Laboratory, 2 allée Louise et Victor Champier BP 30329, 59056 Roubaix, France. [3]Université de Lille, Nord de France, 59000 Lille, France. [4]College of Textile and Clothing Engineering, Soochow University, Suzhou 215006, China. [5]Swedish Centre for Resource Recovery, Faculty of Textiles, Engineering and Business, University of Borås, 50190 Borås, Sweden. ✉email: mohammad_neaz.morshed@hb.se

1

ways including redox reactions (Eq. 1), dehydrogenation reactions (Eq. 2), electrophilic addition to π systems (Eq. 3) and so on[12,13].

$$^.OH + RX \rightarrow RX^{+.} + OH^- \tag{1}$$

$$RH + ^.OH \rightarrow ^.R + H_2O \tag{2}$$

$$RHX + ^.OH \rightarrow RHX(OH) \tag{3}$$

Ferrous ions consumed during the Fenton reaction are regenerated by further reaction of ferric ions with hydrogen peroxide, as in Eqs. 4–6[14].

$$Fe^{2+} + H_2O_2 \rightarrow Fe^{3+} + OH^- + ^.HO \tag{4}$$

$$Fe^{3+} + H_2O_2 \rightarrow Fe^{2+} + H^+ + HO_2^. \tag{5}$$

$$Fe^{3+} + HO_2^. \rightarrow Fe^{2+} + O_2 + H^+ \tag{6}$$

Although Fenton and Fenton-like treatments have noteworthy benefits[15–18], homogeneous Fenton process containing free reagents (iron ions and hydrogen peroxide) have some critical disadvantages including selective reaction conditions (acidic pH), generation of a high amount of iron sludge and single-use reagent which is costly and counterproductive[19,20]. Therefore, much effort has been invested to improve the treatment efficiency of the Fenton reaction process as well as extending their working conditions and cutting down on secondary pollution[21,22].

Heterogeneous Fenton process using various types of catalysts such as zero-valent iron (ZVI = Fe⁰)[23–26], goethite (–FeOOH)[27,28], and Fe_3O_4[29–31], has been extensively studied for pollutant degradation processes. Solid zero-valent iron allows a reduction in iron use, with the potential prospect to work in an operational pH. According to Xu et al.[32], the zero-valent iron-based Fenton-like system provides better degradability of phenolic compounds even in working pH condition (pH 5–6). However, this process still produces iron sludge (due to the agglomeration of particles and limited recyclability of iron due to easy oxidation) as in homogeneous Fenton process. Hence, researchers introduce immobilization of zerovalent iron particles on solid supports to control the sludge formation and ensure reusability of the catalysts. Our recent studies reported the successful immobilization of zerovalent iron nanoparticles on high porosity support material (fibrous polyester fabric) and explored their effectiveness as a fibrous catalyst toward the removal of various organic and pathogenic contaminants in water through a heterogeneous Fenton process without generating secondary pollutants (iron sludge)[33].

In general, the Fenton process is influenced by many factors including, the pH of the reaction medium, the temperature, the hydrogen peroxide concentration and the amount of catalyst which is needed to optimize this process for assessing their measurable performances[34]. Conventional optimization process was determined through the interaction of the individual factors at-a-time while keeping all other conditions constant, this approach does not take into account cross-effects from the factors considered and leads to a poor optimization result[35]. When a multifactor system is present, it is more appropriate to employ statistical-based optimization strategies to achieve such a goal[36]. An experimental design methodology is a modern approach, which has been widely used in several applications[1,37,38] also allowing the modeling of the process. In fact, the design of experiments (DoE) is used to identify or screen the important factors affecting a process or product and to develop statistically significant empirical models[35,39,40]. To our best knowledge, no study has reported the statistical modeling and optimization of heterogeneous Fenton-like removal of organic pollutant using fibrous catalysts through a full factorial design.

Therefore, in this study, an L^{27} full factorial experimental design was used to optimize the removal process of organic pollutants (dye) by a heterogeneous Fenton-like process. Individual and interaction effects of pH and concentration of hydrogen peroxide $[H_2O_2]_{ul}$ was studied in a form of statistical modeling. The responses considered were the reduction of dye concentration (%) after oxidation. Three different catalysts (based on the preparation process) chosen for this study were from our newly developed fibrous catalysts (PET–NH₂–Fe|PET–Si–NH₂–Fe|PET–SH–Fe)[20]. Electrokinetic and X-ray photoelectron spectroscopy (XPS) analysis of resultant materials were also studied. Synthesis and structural analysis of zerovalent iron nanoparticles, formation of Fe^{2+}, reactive species and detailed mechanism of dye removal can be found in our previous studies[20,33].

Experimental

Materials. Analytical grade polyamidoamine-PAMAM dendrimer, 3-(aminopropyl)triethoxysilane (APTES), 1-thioglycerol (SH), ammonium hydroxide (NH₄OH); absolute ethanol (Et-OH); sodium borohydride (NaBH₄), crystal violet (CV), hydrogen peroxide (H₂O₂, 30% w/v) and iron nitrate (Fe(NO)₃) were purchased from Sigma Aldrich Ltd and used as received without any further purifications. Deionized water from Milli-Q® Direct 8 water purification system was used throughout all experiments. The polyester nonwoven membrane used in this study was fabricated in The Swedish School of Textiles (University of Borås) based on a web of cylindrical polyethylene terephthalate fibres (average diameter 12 µm) formed by carding and consolidated by needle punching. The physical characteristics of the fabricated nonwoven are displayed in Table S1.

Catalyst	Factors	Level			Response
		A	B	C	
PET–NH₂–Fe	pH (X1)	5	7	9	Dye Conc., Q_e (%)
	$[H_2O_2]_{\mu l}$ (X2)	100	300	500	Dye Conc., Q_e (%)
PET–Si–NH₂–Fe	pH(X1)	5	7	9	Dye Conc., Q_e (%)
	$[H_2O_2]_{\mu l}$ (X2)	100	300	500	Dye Conc., Q_e (%)
PET–SH–Fe	pH(X1)	5	7	9	Dye Conc., Q_e (%)
	$[H_2O_2]_{\mu l}$ (X2)	100	300	500	Dye Conc., Q_e (%)

Table 1. Matrix of experiment's factors, their levels and response. Q^e concentration of pollutant at equilibrium.

Preparation and chemical grafting of PAMAM, APTES, SH on polyester nonwoven fabrics.

Polyester nonwoven fabrics underwent multi-step surface functionalization process includes, (a). Plasma activation of polyester surface, (b) Chemical grafting of crosslinkers (PAMAM dendrimer, APTES and SH) and (c) Loading of zerovalent iron nanoparticles through in-situ reduction and immobilization as explained in our previous articles[20,33]. Typically, air atmospheric plasma treatment based on dielectric barrier discharge (DBD) was used to activate the polyester surface using a CoatingStar plasma treatment set-up provided by Ahlbrandt System (Germany) at electrical power of 750 W at a speed of 2 m/min.

PAMAM and APTES were chemically grafted using ethanol/water (3:1 v/v) as solvent under constantly stirring for 4 h (PAMAM in air and APTES in N_2 chamber) at 70 °C. Following the same protocol, SH was grafted in N_2 chamber for 12 h. The resulting PET–NH₂, PET–Si–NH₂, and PET–SH were filtered, washed and dried at 60 °C overnight.

Loading of zero-valent iron nanoparticles on polyester nonwoven fabrics.

The immobilization of zerovalent iron nanoparticles (Fe-NPs) on PET–NH₂, PET–Si–NH₂ and PET–SH were achieved using $Fe(NO)_3$ (0.6 wt.%) as precursors and sodium tetrahydroborate (0.9 mM) as a reducing agent. The resultant catalysts, termed as PET–NH₂–Fe, PET–Si–NH₂–Fe, and PET–SH–Fe were mildly washed, vacuum dried and stored in a sealed O_2-free desiccator before further characterization and use.

Material characterizations.

Electrokinetic measurements were carried out to determine the ζ-potential values of fabrics as a function of the pH values of the electrolyte solution (0.001 M KCl). The measurement was carried out using the streaming potential method, in which a liquid is forced to flow through two parallel plates contain samples and streaming potential is generated (Surpass, Anton Paar AB., Sweden). 0.01 M HCl and 0.01 M NaOH were used to adjust the pH values of the electrolyte solution. The **ζ** potential values were calculated using the Helmholtz Smoluchowski equation (Eq. 7).

$$\zeta = \frac{dl\text{str}}{d\Delta p} \times \frac{\eta}{\varepsilon \times \varepsilon_0} \times \frac{L}{A} \qquad (7)$$

where dl/dp is the slope of streaming current vs. differential pressure, η is electrolyte viscosity, ε represents the dielectric coefficient of electrolyte, ε_0 represents permittivity, L is the length of the streaming channel and A is the cross-section of the streaming channel.

X-ray photoelectron spectroscopy (XPS) study was carried out by a spectrophotometer (PHI 5500 ESCA, Physical Electronics INC., USA) equipped with monochromatic aluminium (Al) source (photon energy = 1,486.6 eV). Due to the insufficient conductivity, an electron neutralizer was used to compensate for the charge. Survey scan for the compositional evaluation (Energy range of 0–1,100 eV; Step size of 0.4 eV/step), and the narrow scan for the chemical state analysis with selected range for individual elements and step size of 0.1 eV/step was performed[41–44]. Morphological and structural analysis of such fibrous catalysts were extensively studied in our previous reports[20,33].

Heterogeneous Fenton-like removal of crystal violet dyes.

The heterogeneous Fenton-like removal of crystal violet dye (50 mg/L) using a fibrous catalyst (25 mg/5 mL, PET–NH₂–Fe, PET–Si–NH₂–Fe, and PET–SH–Fe) and H_2O_2 (100–500 µl/5 ml) was investigated in different pH (5, 7, 9) at 22 ± 2 °C. UV/visible spectrophotometer was used to monitor the removal process. Equilibrium time to attain the maximum dye removal has been detected individually for each catalyst. The minimum time required for complete removal of dye using a particular catalyst through an individual set of experiment was considered as equilibrium time. The pH range in this study was estimated based on our previous investigation on same catalysts[20]. The equilibrium concentration (Q_e) of crystal violet solution was measured by referring the absorbance calibration curve of the known standard solution, which allowed calculating the relative dye concentration (%) in the reaction chamber based on initial dye concentration. Based on the relative dye concentration in the chamber at the equilibrium point, the efficiency of the catalysts was estimated through a passive approach.

Design of experiment (DoE) and statistical modeling.

Matrix of the experiment's factors, their levels and response have been presented in Table 1. A full factorial design of experiment combining two factors

RunOrder	PtType	Blocks	Factors		Relative dye concentration, Q_e (%)		
			pH (X1)	[H₂O₂] (X2)	PET–NH₂–Fe	PET–Si–NH₂–Fe	PET–SH–Fe
1	1	1	5	100	0.8070	0.7501	0.7022
2	1	1	5	300	0.4354	0.5101	0.4469
3	1	1	5	500	0.0109	0.0243	0.0228
4	1	1	7	100	0.9625	0.9512	0.9654
5	1	1	7	300	0.8418	0.8626	0.7384
6	1	1	7	500	0.4209	0.4543	0.4481
7	1	1	9	100	0.9412	0.9837	0.9801
8	1	1	9	300	0.9501	0.9402	0.9619
9	1	1	9	500	0.9459	0.9932	0.9454
10	1	1	5	100	0.8319	0.7978	0.6421
11	1	1	5	300	0.4158	0.5498	0.4106
12	1	1	5	500	0.0108	0.0183	0.0208
13	1	1	7	100	0.9572	0.9403	0.9132
14	1	1	7	300	0.8198	0.7806	0.7002
15	1	1	7	500	0.4351	0.4199	0.4278
16	1	1	9	100	0.9803	0.9967	0.9903
17	1	1	9	300	0.9308	0.976	0.9625
18	1	1	9	500	0.9512	0.952	0.9398
19	1	1	5	100	0.8197	0.8212	0.7233
20	1	1	5	300	0.4637	0.4889	0.3606
21	1	1	5	500	0.0103	0.0199	0.0199
22	1	1	7	100	0.9498	0.9731	0.9573
23	1	1	7	300	0.8219	0.8195	0.7498
24	1	1	7	500	0.4664	0.4821	0.4302
25	1	1	9	100	0.9309	0.971	0.9863
26	1	1	9	300	0.9578	0.9804	0.9512
27	1	1	9	500	0.9141	0.9436	0.9607

Table 2. L^{27} full factorial design of experiment based on factors, levels and response data [relative dye concentration at equilibrium (%)].

and three levels for all three fibrous catalysts (PET–NH₂–Fe, PET–Si–NH₂–Fe, and PET–SH–Fe) were chosen. According to the number of control parameters and their levels, a distinct full factorial design has been selected (L^{27}) to determine the optimal number of experiments in triplicates (See Table 2). In the end, a passive response from each trial run in terms of the relative concentration of dye at equilibrium was recorded. The availed results from each trial run are evaluated in "Minitab® 17 graphical and statistical analysis tool" based on main effects, interaction, ANOVA, and a response table.

Results and discussions

The results of this study has been divided into two parts; (1) the first part will discuss the statistical modeling and optimization of the process parameters that affect the mean and variance of the attributes and identify the significant contribution and, (2) the second part will discuss the characterization of fibrous catalyst used in this study.

Part-1: Statistical modeling and optimization of the differences in the process parameters.

Analysis of main effects. The main effect is defined as the effect of an independent variable on a dependent variable averaged across the levels of all independent variable. By analyzing the main effects of the parameters, the general trends of the factor's influence on the process can be determined[45]. Figure 1 shows the main effect plots for the relative dye concentration (%) after Fenton-like oxidation using PET–NH₂–Fe, PET–Si–NH₂–Fe and PET–SH–Fe based on the date shown in Table 2. Results shown in Fig. 1a–c implies that, regardless of the type of the catalysts, with the changing in level in both X1 and X2, the response has significantly altered in a linear model which validates the statistically significant effect of pH and $[H_2O_2]_{ul}$ on the response. Concentration may negatively affect the removal process as explained in various reports[8,20,46,47].

Detailed analysis of the results shows that the lowest level of the factor X1 and highest levels of the factor X2 determined the maximum removal efficiency. With the increase in pH, the net negative surface charges on the catalysts surface cancelling the efficiency of reactive species that are responsible for the removal. Jung et al. (2013) reported that alkaline medium affects both reagents in the Fenton process causing instability in hydrogen peroxide and forming oxides on iron which significantly hinder the general of reactive species[22]. Lower concertation of hydrogen peroxide is too concentrated to react with mineralized iron to produce reactive species. However,
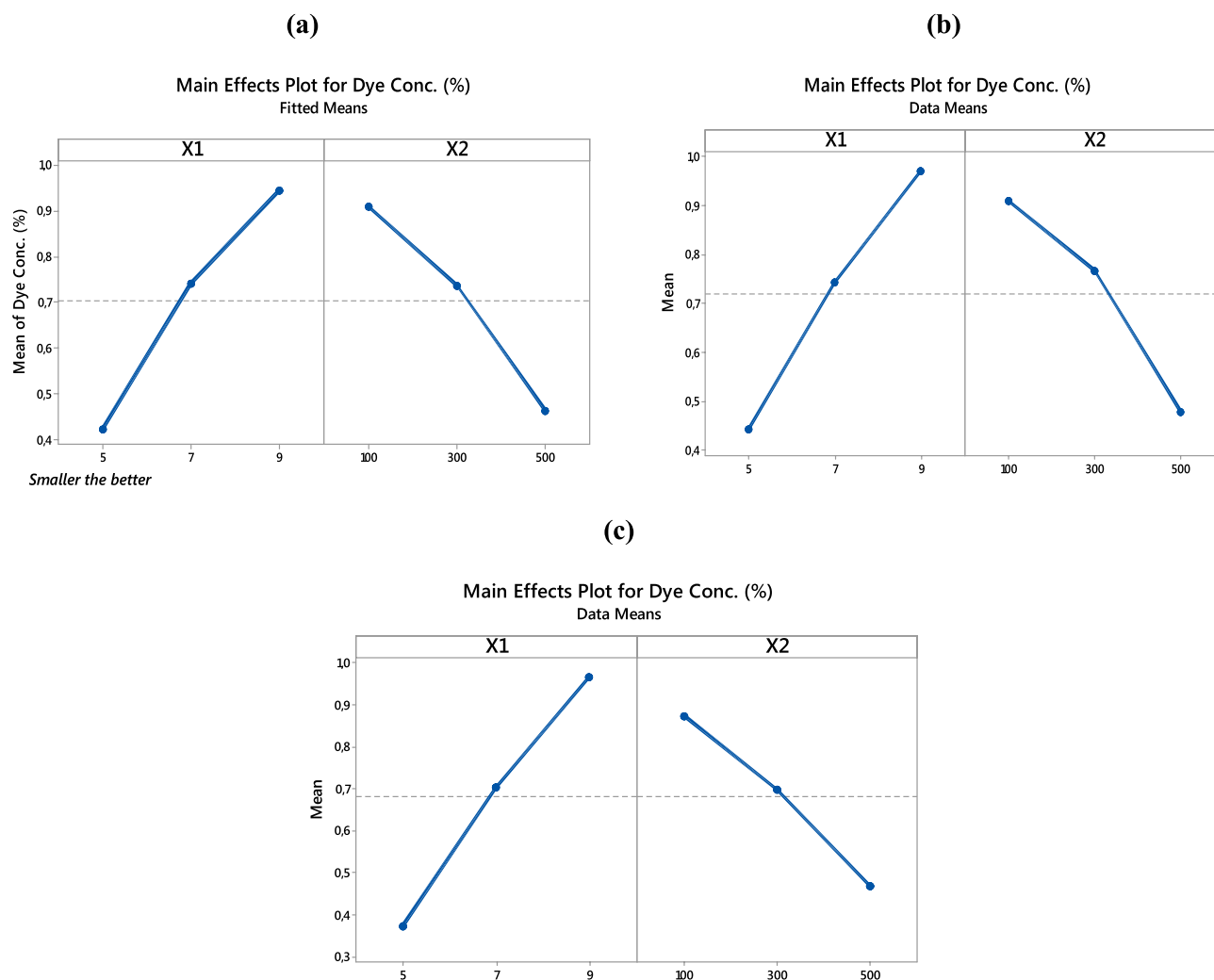
(a)

Main Effects Plot for Dye Conc. (%)
Fitted Means

Smaller the better

(b)

Main Effects Plot for Dye Conc. (%)
Data Means

(c)

Main Effects Plot for Dye Conc. (%)
Data Means

Figure 1. Main effect plots for dye conc. (%) of (**a**) PET–NH$_2$–Fe, (**b**) PET–Si–NH$_2$–Fe and (**c**) PET–SH–Fe; Smaller the better ; [Response: Dye concentration (%)].

it also needs to be noted that, after the saturation concentration of reactants, a further increase in concentration may negatively affect the removal process as explained in various reports[8,20,46,47].

Analysis of interaction effects between factors. Figure 2 shows the interaction effects of the factors in the low level and the high level of another factor. Figure 2a shows the interaction plots for PET–NH$_2$–Fe for the factors pH and [H$_2$O$_2$]$_{\mu l}$. It can be seen that the interactions between X1$_{A \times B}$ and X2 $_{B \times C}$ have significance among factors (see Fig. 2a). The remaining interaction X1$_C$ and X2$_A$ show near straight effect, forming a parallel-like line, meaning these two conditions do not have a relation. On the contrary, the interaction between X1$_A$ and X2$_C$ has shown the most significant relationship. According to Hu, J. et al. (2019), an interaction exists if the relationship is represented by nonparallel lines while parallel lines denote no relationship between the parameters[47]. The interaction plots of other samples (PET–Si–NH$_2$–Fe and PET–SH–Fe) show similar trends like PET–NH$_2$–Fe (See Fig. 2b,c). The overall scenario concludes that the removal efficiency increases with the increase in the concentration of hydrogen peroxide [H$_2$O$_2$] at the same time decrease in pH also increases removal efficiency as consistent with main effects. This also indicates that the interaction plots are suitable for exploring the process parameters.

Analysis of variance-ANOVA. The main effect and interaction plots provide the optimal levels of each factor but do not indicate which factor has the most significant impact on the output and the contribution of each factor. This was determined by the ANOVA, which is a robust method to determine the contribution of each factor and the significance of the optimization model[48]. It is accomplished by determining the Fischer's test value (F-value) and the sum of squares, which are used to evaluate the significance of the parameters; p values below 0.05 or 5% were considered statistically significant[49]. Tables 3, 4 and 5 shows the ANOVA results for the PET–NH$_2$–Fe, PET–Si–NH$_2$–Fe and PET–SH–Fe, respectively. Results indicate, among the significant parameters, the pH has a large influence on the efficiency of the removal with an F-value of 2045.59, 866.65 and 1314.62
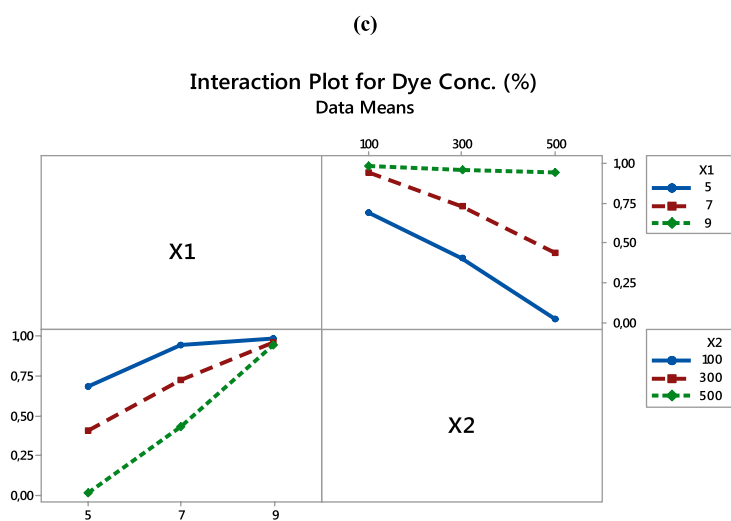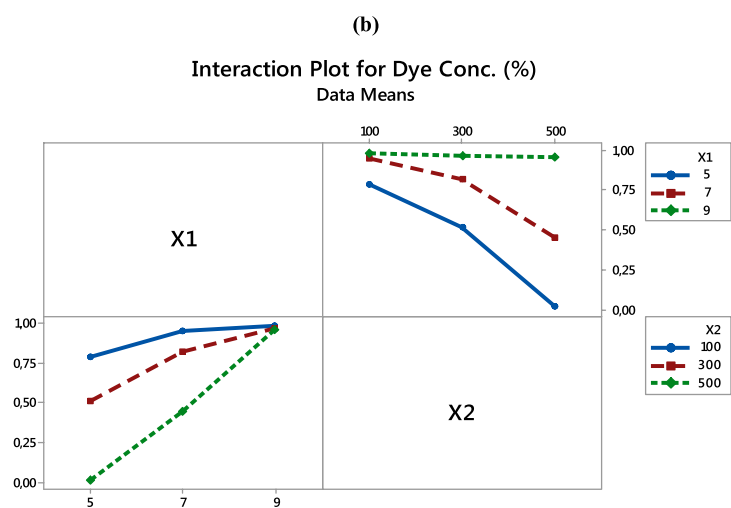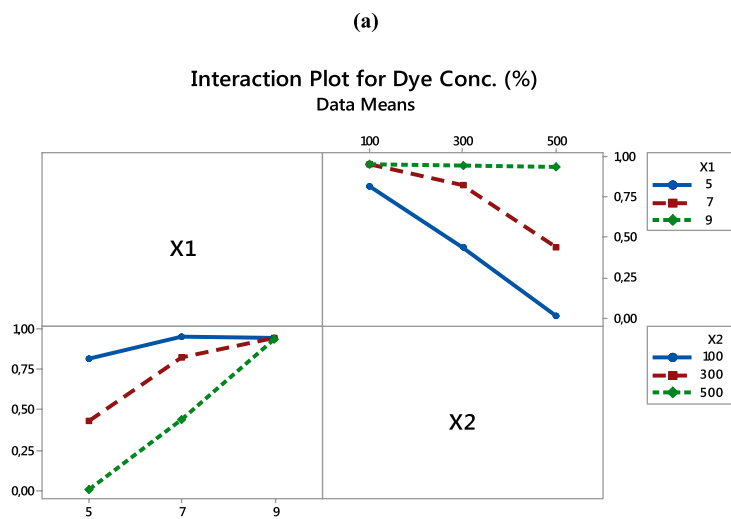
(a)

(b)

(c)

Figure 2. Interaction plots for dye conc. (%) of (**a**) PET–NH$_2$–Fe, (**b**) PET–Si–NH$_2$–Fe and (**c**) PET–SH–Fe [Response : Dye concentration (%)].

Source	DF	Seq SS	p%	Adj SS	Adj MS	F-value	p-value	Remarks
Model	8	2.66076	99.79	2.66076	0.332595	1,092.32	0.000	Significant
Linear	4	2.15717	80.91	2.15717	0.539293	1771.17	0.000	Significant
X1	2	1.24570	46.72	1.24570	0.622849	2045.59	0.000	Significant
X2	2	0.91147	34.19	0.91147	0.455737	1,496.75	0.000	Significant
2-Way interactions	4	0.50359	18.89	0.50359	0.125897	413.48	0.000	Significant
X1*X2	4	0.50359	18.89	0.50359	0.125897	413.48	0.000	Significant
Error	18	0.00548	0.21	0.00548	0.000304			

Table 3. Analysis of variance-ANOVA for dye conc. (%) [PET–NH$_2$–Fe].

Source	DF	Seq SS	p%	Adj SS	Adj MS	F-value	p-value	Remarks
Model	8	2.58356	99.49	2.58356	0.322945	442.61	0.000	Significant
Linear	4	2.13239	82.12	2.13239	0.533098	730.63	0.000	Significant
X1	2	1.26468	48.70	1.26468	0.632338	866.65	0.000	Significant
X2	2	0.86772	33.42	0.86772	0.433858	594.62	0.000	Significant
2-Way interactions	4	0.45117	17.37	0.45117	0.112793	154.59	0.000	Significant
X1*X2	4	0.45117	17.37	0.45117	0.112793	154.59	0.000	Significant
Error	18	0.01313	0.51	0.01313	0.000730			

Table 4. Analysis of variance-ANOVA for dye conc. (%) [PET–SI–NH$_2$–Fe].

Source	DF	Seq SS	p%	Adj SS	Adj MS	F-value	p-Value	Remarks
Model	8	2.65499	99.59	2.65499	0.331873	550.48	0.000	Significant
Linear	4	2.32752	82.31	2.32752	0.581880	965.17	0.000	Significant
X1	2	1.58511	59.46	1.58511	0.792555	1,314.62	0.000	Significant
X2	2	0.74241	27.85	0.74241	0.371205	615.72	0.000	Significant
2-Way interactions	4	0.32747	12.28	0.32747	0.081867	135.79	0.000	Significant
X1*X2	4	0.32747	12.28	0.32747	0.081867	135.79	0.000	Significant
Error	18	0.01085	0.41	0.01085	0.000603			

Table 5. Analysis of variance-ANOVA for dye conc. (%) [PET–SH–Fe].

and a p-value of 0.000 (same for all three) for ET–NH$_2$–Fe, PET–Si–NH$_2$–Fe and PET–SH–Fe, respectively. The concentration of hydrogen peroxide [H$_2$O$_2$] is also significant (p = 0.000) but has a lower influence than that of pH with F-values of 1496.75, 594.62 and 615.72, respectively. The model summary shows strong correlation as expressed by R^2 value over 98% for all three catalysts (see Tables S2, S4, S6). On the other hand, by comparing the F-values among three fibrous catalysts considering all factors and levels, it can be seen that the type of catalyst does not have any significant impact on the dye removal. The 2-way interaction of the factors also shows an overall significant impact on dye removal. However, extensive analysis (see Tables S3, S5, S7) showing coefficient of each interaction identifies the interaction between X1$_B$ and X2$_A$ as not significant in PET–Si–NH$_2$–Fe (see Table S5), X1$_A$ and X2$_B$ plus X1$_B$ and X2$_B$ in PET–SH–Fe (see Table S7).

The influence of each factor is also expressed as the percent contribution (p%). From the results, it can be seen that pH has the percent contribution of 46.72% in PET–NH$_2$–Fe, 48.70% in PET–Si–NH$_2$–Fe and 51.46% in PET–SH–Fe, followed by the [H$_2$O$_2$]$_{ul}$ where 34.19% in PET–NH$_2$–Fe, 33.42% in PET–Si–NH$_2$–Fe and 27.456% in PET–SH–Fe was recorded. These findings indicate that, although both factors have significant influence over the dye removal efficiency, pH has a higher influence than that of [H$_2$O$_2$]$_{ul}$. Seq. SS, Adj. SS, Adj. MS values are in line with f-values of all fibrous catalysts and all factors. A detailed study among three catalysts indicates that the influences of the pH are greatly affecting on by PET–SH–Fe followed by PET–Si–NH$_2$ and PET–NH$_2$–Fe whereas the influence of [H$_2$O$_2$]$_{ul}$ largely in PET–NH$_2$–Fe followed by PET–Si–NH$_2$–Fe and PET–SH–Fe catalyst. The prominent effect of pH over [H$_2$O$_2$]$_{ul}$ can be explained by the synergic effect of pH on stabilization of hydrogen peroxide and formation of reactive species, which ultimately performs the removal of dyes, in an unlikely pH condition the no removal occurs, whereas in a favourable pH condition, lower or higher concentration of [H$_2$O$_2$]$_{ul}$ will affect the removal but will not be absent[46,50].
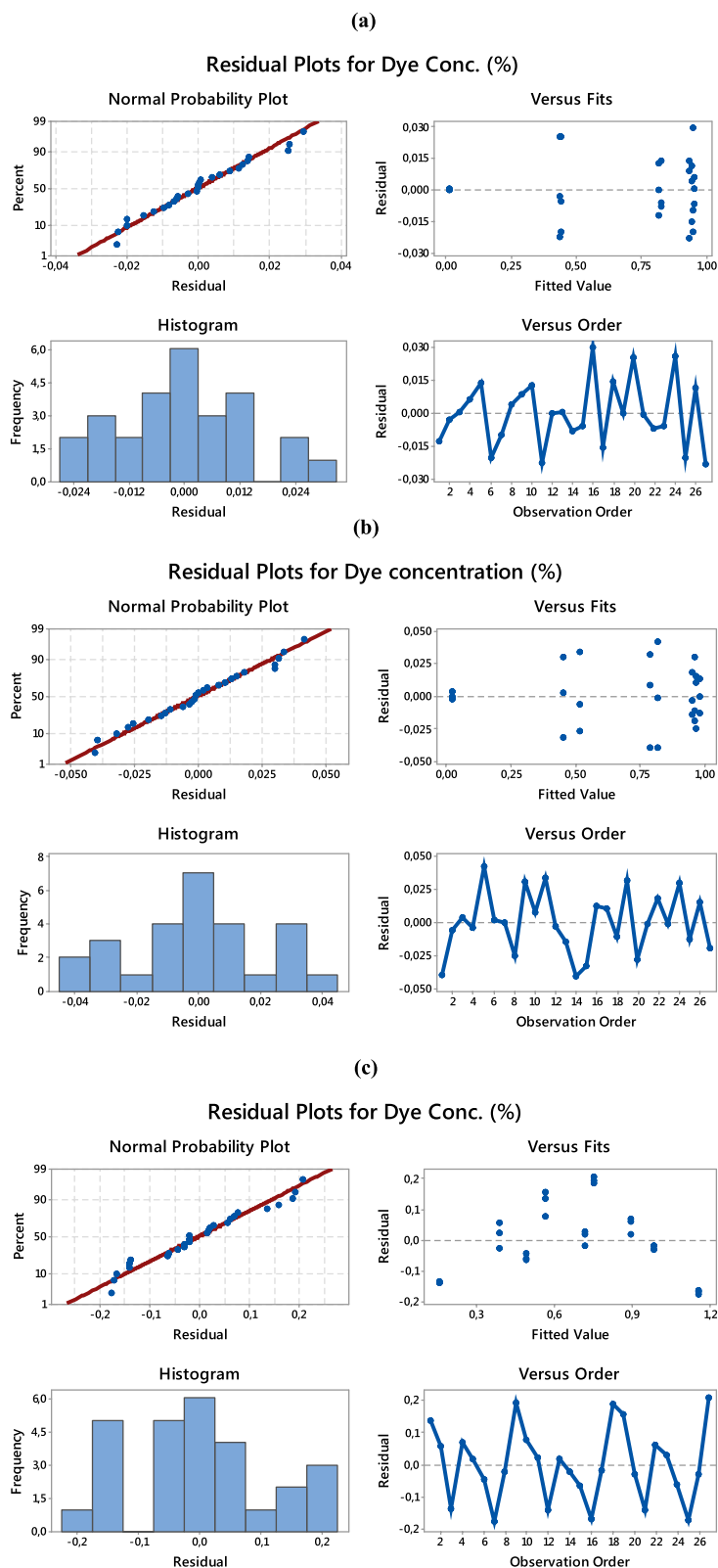
(a)

Residual Plots for Dye Conc. (%)

(b)

Residual Plots for Dye concentration (%)

(c)

Residual Plots for Dye Conc. (%)

Figure 3. Residual plots for dye conc. (%) (**a**) PET–NH$_2$–Fe, (**b**) PET–Si–NH$_2$–Fe and (**c**) PET–SH–Fe.

Analysis of residual plots. Figure 3a–c shows the residual plots for dye concentration (%) for PET–NH$_2$–Fe, PET–Si–NH$_2$–Fe and PET–SH–Fe fibrous catalysts, respectively. The four plots of normal probability, residuals versus the fitted values, the histogram, and the residuals versus the observation order are shown in Fig. 3. From

(a)

Individual Value Plot of Dye Conc. (%)
95% CI for the Mean

Individual standard deviations were used to calculate the intervals.

(b)

Individual Value Plot of Dye Conc. (%)
95% CI for the Mean

Individual standard deviations were used to calculate the intervals.

(c)

Interval Plot of Dye Conc. (%)
95% CI for the Mean

Individual standard deviations were used to calculate the intervals.
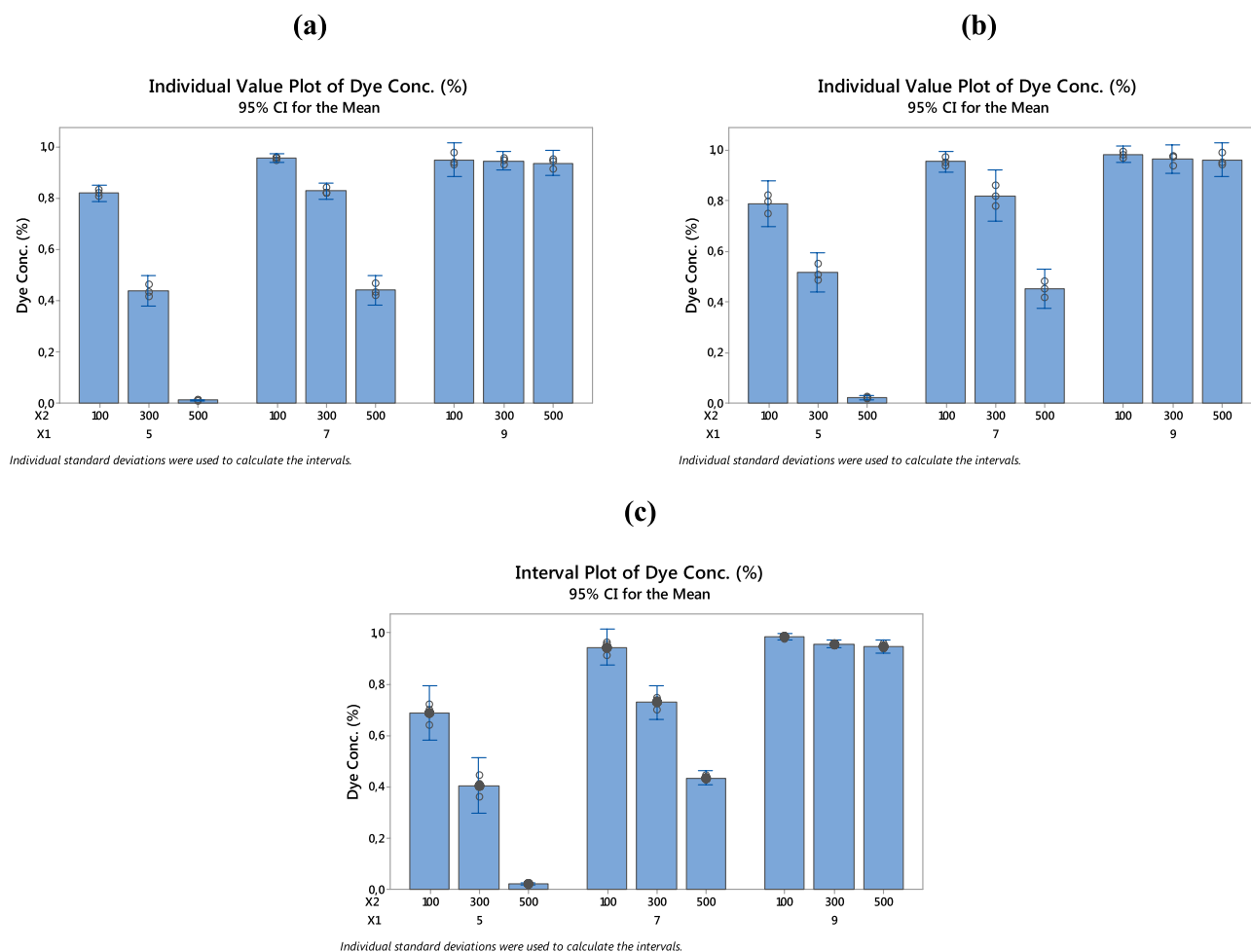
Figure 4. Individual value plots for dye conc. (%); (**a**) PET–NH$_2$–Fe, (**b**) PET–Si–NH$_2$–Fe and (**c**) PET–SH–Fe.

Fig. 3a, it is evident that the normal probability plot exhibits a nearly linear response, demonstrating that the errors are distributed normally. This is confirmed by the histogram, which also shows a normal distribution. The plot of the residuals versus the fitted values indicates that the residuals are randomly distributed around the zero lines, indicating that no sequential association exists and the errors have a constant variance. Moreover, the plot of the residuals versus the observation order is used to evaluate the pattern that may have an impact on the output. It is observed that the residuals are normally distributed close to the zero lines, which implies that there is a fair association with the parameters that do not require any further analysis of the errors[51–53]. A similar trend has been found in Fig. 3b,c.

Analysis of individual value plots. Because individual value plots display all values for all groups at the same time, they are especially helpful when the study is dealing with variables, groups, and even subgroups. The individual value plot of dye concentration (%) after oxidation with PET–NH$_2$–Fe, PET–SI–NH$_2$–Fe and PET–SH–Fe fibrous catalysts, has been plotted for each factor and their levels (see Fig. 4). A close look at all the figures shows that there is a similar trend in all samples indicating the sample type does not influence the response. However, from Fig. 1a it can clearly be seen that both pH and [H$_2$O$_2$]$_{\mu l}$ affect the results significantly. With lower pH, all concentration of [H$_2$O$_2$]$_{\mu l}$ gives a nominal removal performance, whereas the highest concentration of [H$_2$O$_2$]$_{\mu l}$ gives the best efficiency. On the other hand, in pH-7 the efficiency disrupted significantly by more than 50%. And finally, in the highest level of pH, there is no removal recorded regardless of the change in concentration of hydrogen peroxide. The same explanation corresponds to the other catalysts samples. These results provide significant statistical evidence to predict the best possible parameters and their levels.

Analysis of fitted line plots. Figure 5a–c shows the fitted plots of the predicted versus the actual values for the responses for PET–NH$_2$–Fe, PET–Si–NH$_2$–Fe and PET–SH–Fe fibrous catalysts, respectively. It can be observed that the points reflect the deviation of the actual values from the predicted or fitted values. The graph indicates that the model is significant because the residuals are close to the diagonal line. In addition, the Pearson correlation coefficient between the predicted and actual values for the responses was 1.000 with a p-value of 0.000, which indicates a strong relationship between the predicted and actual values for all three fibrous catalysts[54,55].
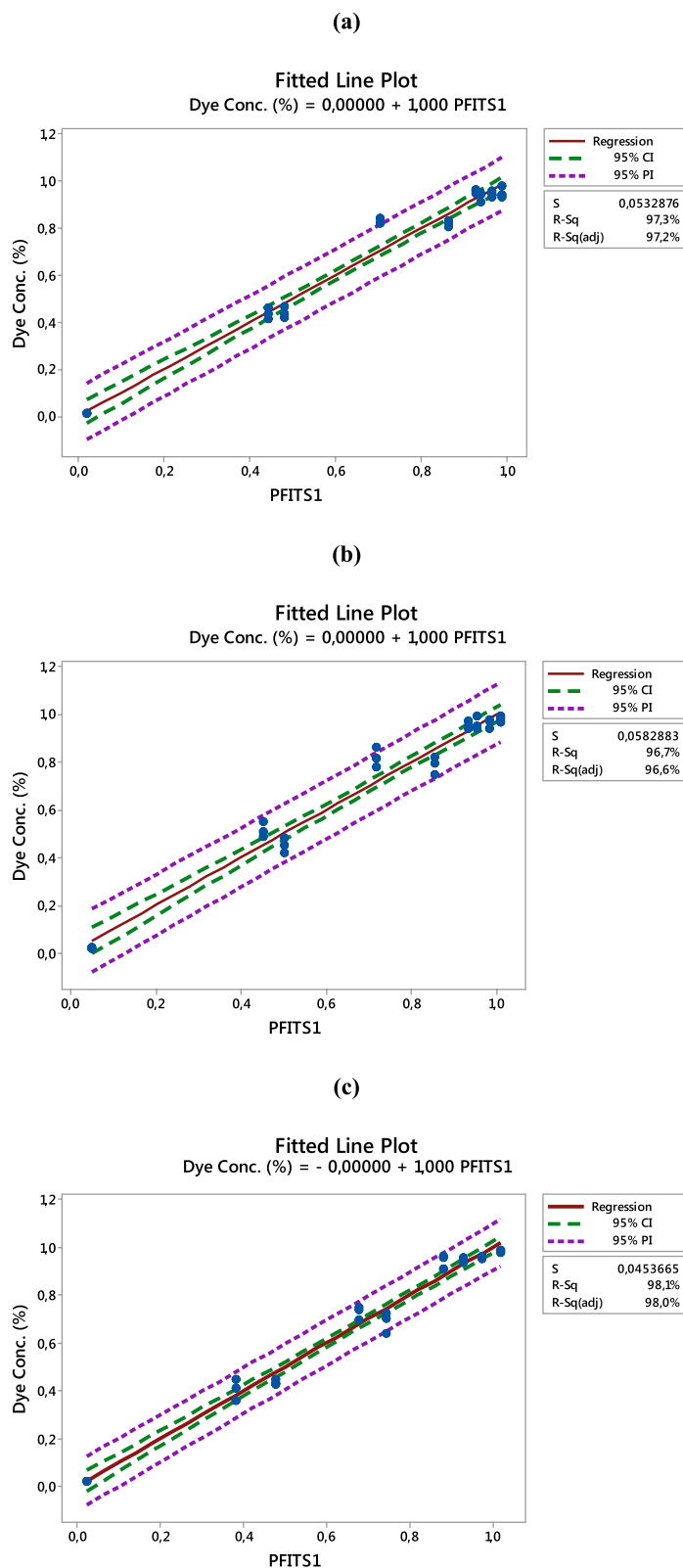
(a)

(b)

(c)

Figure 5. Fitted plots for dye Conc. (%); (**a**) PET–NH$_2$–Fe, (**b**) PET–Si–NH$_2$–Fe and (**c**) PET–SH–Fe.

Part-2: Characterization of fibrous catalysts. *Electrokinetic measurement (ζ-potential analysis).* The isoelectric point (iep = pH|ζ = 0) can be determined through the **ζ**-potential values of untreated, plasma-treated and iron-loaded polyester fabrics that has been observed by electrokinetics and measured as streaming potential.
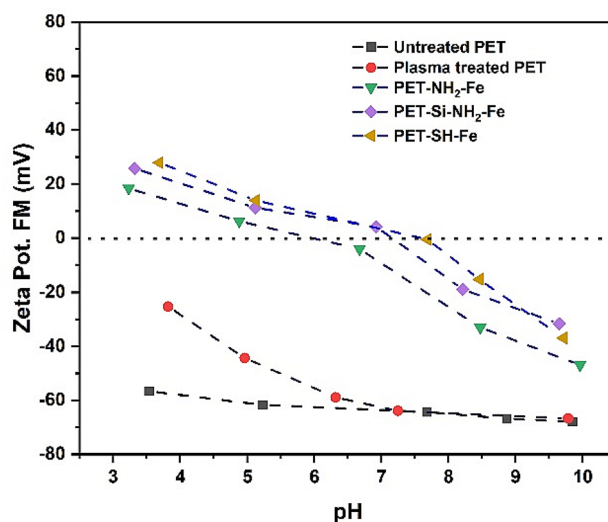
Figure 6. The ζ-potential value of samples as a function of the pH of the electrolyte solution (0.001 M KCl).

The summary of the **ζ**-potential analysis of the samples is displayed in Fig. 6. It can be seen that the isoelectric point of untreated polyester fibres is pH = 3.9 which means that negative surface charge will be observed for the polyester fibres for pH higher than 3.9. Due to the further addition of –OH and –COOH groups during plasma treatment of the PET fibres (PET), the surface charge and isoelectric point were further negative starting from − 6.89 mV at pH = 3.45 to until − 49.23 mV at pH = 9.91 (see Fig. 6). With a negative surface containing –OH and –COOH groups may pose an ideal environment for robust electrostatic incorporation of cationic iron ions (Fe^{3+}) followed by reduction and immobilization into polyester fabrics. Upon incorporation of Fe^0, the isoelectric point of PET–NH_2–Fe, PET–Si–NH_2–Fe and PET–SH–Fe shifted to pH around 7 signifies (see Fig. 6) an increase in **ζ**-potential which can be due to the loading of iron particles and reduction of oxygen-containing groups.

X-ray photoelectron spectroscopy (XPS).   The element composition and the nature of the chemical bonding of a plasma treated PET and PET-NH_2-Fe were evaluated by XPS (see Fig. 7 and Fig. S2 of supplementary information). Results summarized in Table 6 shows that a control sample contains 76.4 a.t% carbon and 21.1 a.t% oxygen, which after plasma activation changed into 75.4 a.t% carbon and 24.6 a.t% oxygen indicating an increase in oxygen due to formation of –COOH and –OH groups on the fibre surface. After the modification of the fabric with PAM (PET–NH_2), nitrogen was detected in the surface composition having and iron was detected on PET–NH_2–Fe sample.

A detailed study of Fig. 7b (plasma-treated sample) illustrates that the sample consists mainly of C and O in a ratio around 3:1. Majority of the carbon (i.e. 60% of the area) refers to the C≡C and C=C bonding type in the hydrocarbon chain, whereas 40% of the area corresponds to C=O, C–O and COO⁻. O1s, on the other hand, shows 90% of the signal area is for C=O, C–O and –OH. All features in the O1s and part of C1s correspond to polyester, i.e. the COO⁻ functional group. Figure 7c and Fig. S2d shows the presence of 7.4 at.% nitrogen that confirms the grafting of PAM is mainly a graphitic-N type (R_3N) and the rest refers to pyrrolic (R_2NH). C–O proportion is enriched in C1s and O1s peaks. Figure 7d and Fig. S2f indicates that the sample consists of 5.0 at.% Fe in Fe(III) state. 2.3 at.% N at 400.0 eV corresponds to a 100% pyrrolic-N, secondary amine and/or primary amide condition, i.e. C_4H_9N/R_2NH/$RCONH_2$). The C–O ratio is around 2:1. Alkane-type hydrocarbon chain, i.e. C1s = 284.8 eV (C–C) is determined. Rest of the C signal can be assigned to the carboxylic group, i.e. COO⁻. Moreover, most of the deconvoluted peaks in O1s also agrees with the features in a carboxylic group. In addition, a deconvoluted located at 529.5 eV corresponds to metal, could be metal-Fe (zerovalent iron).

Conclusions

A full factorial design of experiment to predict and optimize the heterogeneous Fenton-like removal of organic pollutants using newly developed fibrous catalysts has been successfully achieved. The statistical insight on the effect of the factors (X1 and X2) and their levels in the removal process has been identified. Primarily, the statistical model showed that for both factors (X1 and X2) optimum values for the process variables exist. The results have been summarized below.

a) Optimum operating conditions were determined based on a mathematical model in the form of statistical modeling, they are: initial acidic pH of 5, [H_2O_2]$_{\mu l}$ of 500 µl which is a distinctive behaviour in the heterogeneous Fenton-like process. Under these conditions, 99% of pollutants are being removed in a rapid oxidation reaction.
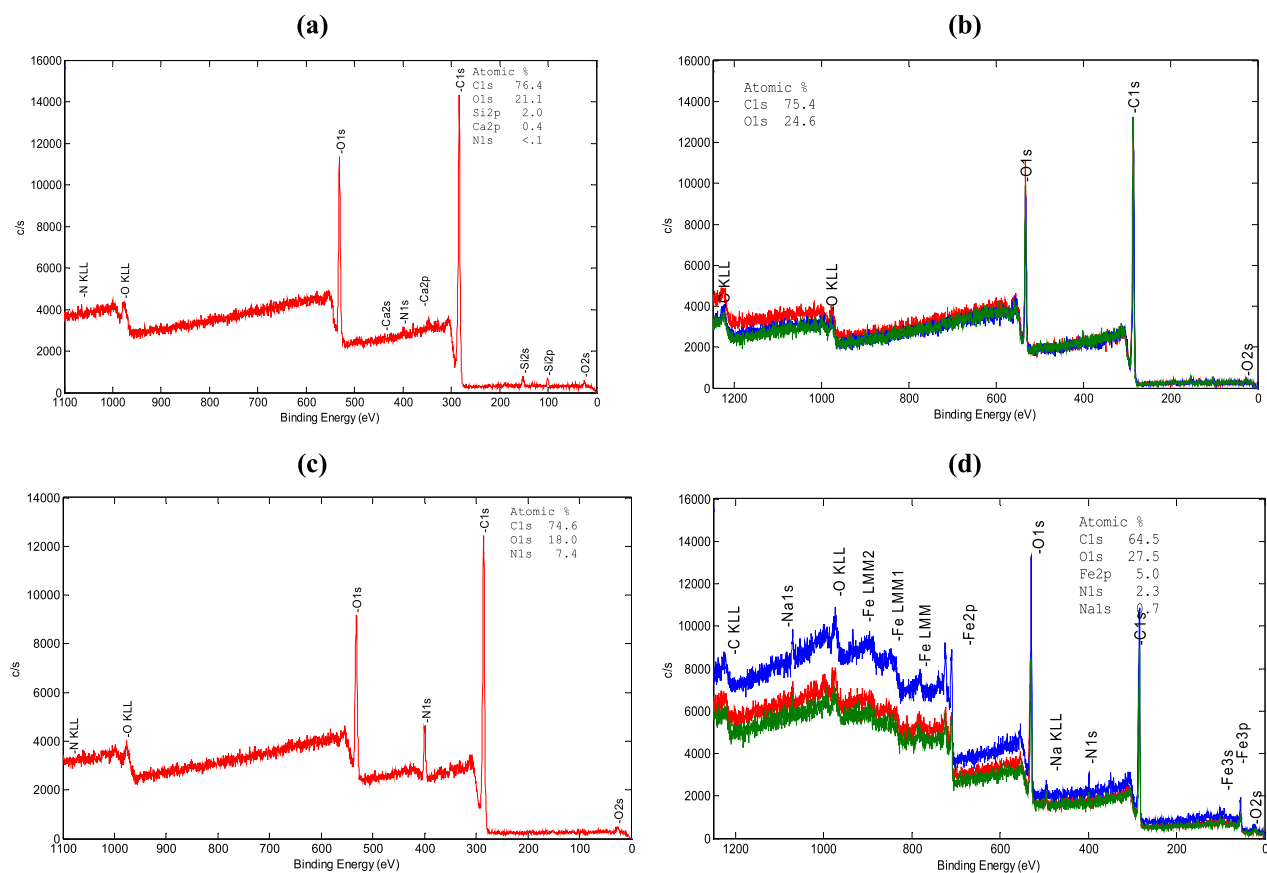
Figure 7. Wide scan XPS spectra of (**a**) untreated PET, (**b**) Plasma treated PET, (**c**) PET–NH_2 and (**d**) PET–NH_2–Fe.

Sample	C (a.t %)	O (a.t %)	N (a.t %)	Fe (a.t %)
Untreated PET	76.4	21.1	< 0.1	0
Plasma treated PET	75.4	24.6	0	0
PET–NH_2	74.6	18.0	7.4	0
PET–NH_2–Fe	64.5	27.5	2.3	5.0

Table 6. Atomic proportion (a.t%) of the surface chemical composition of the samples.

b) The interaction between X1 and X2 was of statistical significance with respect to the lower level of X1 and a higher level of X2 whereas the X1 turned into the key factor for the process. Whereas the type of catalysts turned out to be statistically insignificant.

c) The ANOVA results provided evidence of the statistical significance of the factors and their corresponding levels that gives clear information during optimizing the process productivity and effective prediction.

d) The ζ-potential and XPS analyses of the fibrous catalysts validated the surface modification of polyester fabric and loading of zerovalent iron nanoparticles.

While providing valuable insight into the roles of factors, the model provides rational ground to undertake a kinetic model that will further provide an in-depth understanding of the mechanisms and kinetics of the heterogeneous Fenton-like removal of complex pollutants in wastewater using such catalysts.

References

1. Ramirez, J. H., Costa, C. A. & Madeira, L. M. Experimental design to optimize the degradation of the synthetic dye Orange II using Fenton's reagent. *Catal. Today* **107**, 68–76 (2005).

2. Clara, M. *et al.* Removal of selected pharmaceuticals, fragrances and endocrine disrupting compounds in a membrane bioreactor and conventional wastewater treatment plants. *Water Res.* **39**, 4797–4807 (2005).
3. Pervez, M., He, W., Zarra, T., Naddeo, V. & Zhao, Y. New sustainable approach for the production of Fe_3O_4/graphene oxide-activated persulfate system for dye removal in real wastewater. *Water* **12**, 733 (2020).
4. Mushtaq, F., Chen, X., Torlakcik, H. et al. Enhanced catalytic degradation of organic pollutants by multi-stimuli activated multiferroic nanoarchitectures. *Nano Res.* **13**, 2183–2191 (2020).
5. Malik, P. & Saha, S. Oxidation of direct dyes with hydrogen peroxide using ferrous ion as catalyst. *Sep. Purif. Technol.* **31**, 241–250 (2003).
6. Hou, H., Zeng, X. & Zhang, X. 2D/2D heterostructured photocatalyst: Rational design for energy and environmental applications. *Sci. China Mater.* https://doi.org/10.1007/s40843-019-1256-0 (2020).
7. Ye, Y. *et al.* Remarkable surface-enhanced Raman scattering of highly crystalline monolayer Ti_3C_2 nanosheets. *Sci. China Mater.* **63**, 794–805 (2020).
8. Pignatello, J. J., Oliveros, E. & MacKay, A. Advanced oxidation processes for organic contaminant destruction based on the Fenton reaction and related chemistry. *Crit. Rev. Environ. Sci. Technol.* **36**, 1–84 (2006).
9. Feng, Y. *et al.* Self-powered electrochemical system by combining Fenton reaction and active chlorine generation for organic contaminant treatment. *Nano Res.* **12**, 2729–2735 (2019).
10. Babuponnusami, A. & Muthukumar, K. A review on Fenton and improvements to the Fenton process for wastewater treatment. *J. Environ. Chem. Eng.* **2**, 557–572 (2014).
11. Pervez, M. *et al.* Efficient degradation of mordant blue 9 using the fenton-activated persulfate system. *Water* **11**, 2532 (2019).
12. Nidheesh, P. Heterogeneous Fenton catalysts for the abatement of organic pollutants from aqueous solution: A review. *RSC Adv.* **5**, 40552–40577 (2015).
13. Huang, C., Dong, C. & Tang, Z. Advanced chemical oxidation: Its present role and potential future in hazardous waste treatment. *Waste Manage.* **13**, 361–377 (1993).
14. Morshed, M. N., Bouazizi, N., Behary, N., Guan, J. & Nierstrasz, V. Stabilization of zero valent iron (Fe0) on plasma/dendrimer functionalized polyester fabrics for Fenton-like removal of hazardous water pollutants. *Chem. Eng. J.* **374**, 658–673 (2019).
15. Babuponnusami, A. & Muthukumar, K. Degradation of phenol in aqueous solution by fenton, sono-fenton and sono-photo-fenton methods. *Clean-Soil Air Water* **39**, 142–147 (2011).
16. Chen, D. *et al.* Heterogeneous Fenton-like catalysis of Fe-MOF derived magnetic carbon nanocomposites for degradation of 4-nitrophenol. *RSC Adv.* **7**, 49024–49030 (2017).
17. Ma, Y.-S., Huang, S.-T. & Lin, J.-G. Degradation of 4-nitrophenol using the Fenton process. *Water Sci. Technol.* **42**, 155–160 (2000).
18. Karimi, A., Aghbolaghy, M., Khataee, A. & Bargh, S.S. Use of enzymatic bio-Fenton as a new approach in decolorization of malachite green. *Sci. World J.* **2012**, 691569. https://doi.org/10.1100/2012/691569 (2012).
19. Nidheesh, P. V., Gandhimathi, R. & Ramesh, S. T. Degradation of dyes from aqueous solution by Fenton processes: A review. *Environ. Sci. Pollut. Res.* **20**, 2099–2132 (2013).
20. Morshed, M. N. *et al.* Modification of fibrous membrane for organic and pathogenic contaminants removal: From design to application. *RSC Adv.* **10**, 13155–13173 (2020).
21. Zhang, N., Tsang, E. P., Chen, J., Fang, Z. & Zhao, D. Critical role of oxygen vacancies in heterogeneous Fenton oxidation over ceria-based catalysts. *J. Colloid Interface Sci.* **558**, 163–172 (2020).
22. Jung, Y. S., Park, J-Y., Ko, S-O. & Kim, Y-H. Stabilization of hydrogen peroxide using phthalic acids in the Fenton and Fenton-like oxidation. *Chemosphere* **90**(2), 812–819 (2013).
23. Zhou, T., Li, Y., Ji, J., Wong, F.-S. & Lu, X. Oxidation of 4-chlorophenol in a heterogeneous zero valent iron/H_2O_2 Fenton-like system: Kinetic, pathway and effect factors. *Sep. Purif. Technol.* **62**, 551–558 (2008).
24. Kallel, M., Belaid, C., Mechichi, T., Ksibi, M. & Elleuch, B. Removal of organic load and phenolic compounds from olive mill wastewater by Fenton oxidation with zero-valent iron. *Chem. Eng. J.* **150**, 391–395 (2009).
25. Singh, P. *et al.* Solar-Fenton removal of malachite green with novel Fe0-activated carbon nanocomposite. *Appl. Catal. A* **476**, 9–18 (2014).
26. Deb, H., Morshed, M. N., Xiao, S, Al Azad, S., Cai, Z. & Ahmed, A. Design and development of TiO 2-Fe 0 nanoparticle-immobilized nanofibrous mat for photocatalytic degradation of hazardous water pollutants. *J Mater Sci: Mater Electron* **30**(5), 4842–4854 (2019).
27. de Plata, G. B. O., Alfano, O. M. & Cassano, A. E. Decomposition of 2-chlorophenol employing goethite as Fenton catalyst. I. Proposal of a feasible, combined reaction scheme of heterogeneous and homogeneous reactions. *Appl. Catal. B Environ.* **95**, 1–13 (2010).
28. de la Plata, G. B. O., Alfano, O. M. & Cassano, A. E. Decomposition of 2-chlorophenol employing goethite as Fenton catalyst II: Reaction kinetics of the heterogeneous Fenton and photo-Fenton mechanisms. *Appl. Catal. B* **95**, 14–25 (2010).
29. Costa, R. C., Moura, F. C., Ardisson, J., Fabris, J. & Lago, R. Highly active heterogeneous Fenton-like systems based on Fe0/Fe_3O_4 composites prepared by controlled reduction of iron oxides. *Appl. Catal. B* **83**, 131–139 (2008).
30. Huang, L., Weng, X., Chen, Z., Megharaj, M. & Naidu, R. Synthesis of iron-based nanoparticles using oolong tea extract for the degradation of malachite green. *Spectrochim. Acta Part A Mol. Biomol. Spectrosc.* **117**, 801–804 (2014).
31. Wu, Y. *et al.* Heterogeneous Fenton-like oxidation of malachite green by iron-based nanoparticles synthesized by tea extract as a catalyst. *Sep. Purif. Technol.* **154**, 161–167 (2015).
32. Xu, L. & Wang, J. A heterogeneous Fenton-like system with nanoparticulate zero-valent iron for removal of 4-chloro-3-methyl phenol. *J. Hazard. Mater.* **186**, 256–264 (2011).
33. Morshed, M. N. *et al.* Iron-loaded amine/thiol functionalized polyester fibers with high catalytic activities: A comparative study. *Dalton Trans.* **48**, 8384–8399 (2019).
34. Kahoush, M., Behary, N., Cayla, A. & Nierstrasz, V. Bio-Fenton and Bio-electro-Fenton as sustainable methods for degrading organic pollutants in wastewater. *Process Biochem.* **64**, 237–247 (2018).
35. Elhalil, A. *et al.* Factorial experimental design for the optimization of catalytic degradation of malachite green dye in aqueous solution by Fenton process. *Water Resour. Industry* **15**, 41–48 (2016).
36. Kempthorne, O. *The design and analysis of experiments.* (Wiley, 1952).
37. Smith, E. H. Optimising the design of a piston-ring pack using DoE methods. *Tribol. Int.* **44**, 29–41 (2011).
38. Sukthomya, W. & Tannock, J. The optimisation of neural network parameters using Taguchi's design of experiments approach: An application in manufacturing process modelling. *Neural Comput. Appl.* **14**, 337–344 (2005).
39. Brasil, J. L. *et al.* Factorial design for optimization of flow-injection preconcentration procedure for copper (II) determination in natural waters, using 2-aminomethylpyridine grafted silica gel as adsorbent and spectrophotometric detection. *Int. J. Environ. Anal. Chem.* **85**, 475–491 (2005).
40. Cai, Y., Liang, Y., Navik, R., Zhu, W., Zhang, C., Pervez, M.N., Wang, Q. Improved reactive dye fixation on ramie fiber in liquid ammonia and optimization of fixation parameters using the Taguchi approach. Dyes Pigments 108734 (2020).
41. Moulder, J. F. *Handbook of X-ray photoelectron spectroscopy.* 230–232 (Physical electronics, 1995).
42. Okpalugo, T. I. T., Papakonstantinou, P., Murphy, H., McLaughlin, J. & Brown, N. M. D. High resolution XPS characterization of chemical functionalised MWCNTs and SWCNTs. *Carbon* **43**, 153–161 (2005).

43. Yang, L. *et al.* A new carboxyl-copper-organic framework and its excellent selective absorbability for proteins. *J. Solid State Chem.* **218**, 64–70 (2014).
44. Guo, X., Xu, B., Zhang, W., Cai, Z. & Wen, Z. XPS analysis for cubic boron nitride crystal synthesized under high pressure and high temperature using Li3N as catalysis. *Appl. Surf. Sci.* **321**, 94–97 (2014).
45. Sadeghi, M. M., Modarresnia, A. R. & Shafiei, F. Parameters effects evaluation of microbial strengthening of sandy soils in mixing experiments using taguchi methodology. *Geomicrobiol J* **32**, 453–465 (2015).
46. Duesterberg, C. K. & Waite, T. D. Process optimization of Fenton oxidation using kinetic modeling. *Environ. Sci. Technol.* **40**, 4189–4195 (2006).
47. Hu, J. *et al.* In-situ Fe-doped g-C3N4 heterogeneous catalyst via photocatalysis-Fenton reaction with enriched photocatalytic performance for removal of complex wastewater. *Appl. Catal. B* **245**, 130–142 (2019).
48. Miller, R. G. Jr. *Beyond ANOVA: Basics of Applied Statistics* (CRC Press, New York, 1997).
49. St, L. & Wold, S. Analysis of variance (ANOVA). *Chemometr. Intell. Lab. Syst.* **6**, 259–272 (1989).
50. Lodha, B. & Chaudhari, S. Optimization of Fenton-biological treatment scheme for the treatment of aqueous dye solutions. *J. Hazard. Mater.* **148**, 459–466 (2007).
51. Sudhakara, D. & Prasanthi, G. Parametric optimization of wire electrical discharge machining of powder metallurgical cold worked tool steel using Taguchi method. *J. Inst. Eng. India Series C* **98**, 119–129 (2017).
52. Shafiq, F. *et al.* Structural relationships and optimization of resin-finishing parameters using the Taguchi approach. *Cellulose* **25**, 6175–6190 (2018).
53. Pervez, M., Shafiq, F., Sarwar, Z., Jilani, M. M. & Cai, Y. Multi-response optimization of resin finishing by using a taguchi-based grey relational analysis. *Materials* **11**, 426 (2018).
54. Zhu, X., Tian, J., Liu, R. & Chen, L. Optimization of Fenton and electro-Fenton oxidation of biologically treated coking wastewater using response surface methodology. *Sep. Purif. Technol.* **81**, 444–450 (2011).
55. Arslan-Alaton, I., Yalabik, A. B. & Olmez-Hanci, T. Development of experimental design models to predict Photo-Fenton oxidation of a commercially important naphthalene sulfonate and its organic carbon content. *Chem. Eng. J.* **165**, 597–606 (2010).

Acknowledgements

Author contributions

M.N.M. and V.N. designed the study hypothesis and performed the experimental works. M.N.M., N.B., N.B. M.N.P. and V.A.N. assembled, analyzed and interpreted the data. All authors were involved in writing and revising of the manuscript.

Funding

Competing interests

The authors declare no competing interests.

Additional information

Supplementary information is available for this paper at https://doi.org/10.1038/s41598-020-72401-z.

Correspondence and requests for materials should be addressed to M.N.M.

Reprints and permissions information is available at www.nature.com/reprints.

Publisher's note Springer Nature remains neutral with regard to jurisdictional claims in published maps and institutional affiliations.